References

1. Yamanoue T, Horibe M, Izumi H, Tsuchiya T. Intraoperative coronary artery spasm—retrospective review of ten cases (in Japanese with English abstract). Masui (Jpn J Anesthesiol). 1990;39:376–82.
2. Koshiba K, Hoka S. Clinical characteristics of perioperative coronary spasm: reviews of 115 case reports in Japan. J Anesth. 2001;15:93–9.
3. Maseri A, Davies G, Hackett D, Kaski JC. Coronary artery spasm and vasoconstriction. The case for a distinction. Circulation. 1990;81:1983–91.
4. Yasue H, Kugiyama K. Coronary spasm: clinical features and pathogenesis. Intern Med. 1997;36:760–5.
5. Kugiyama K, Yasue H. Pathophysiology of coronary spasm (in Japanese with English abstract). Nippon Rinsho. 1998;56:2483–7.
6. Tilmant PY, Lablanche JM, Thieuleux FA, Dupuis BA, Bertrand ME. Detrimental effect of propranolol in patients with coronary arterial spasm countered by combination with diltiazem. Am J Cardiol. 1983;52:230–3.
7. Vargas R, Gillis RA, Ramwell PW. Propranolol promotes cocaine-induced spasm of porcine coronary artery. J Pharmacol Exp Ther. 1991;257:644–6.
8. De Cesare N, Cozzi S, Apostolo A, Berti M, Carbucicchio C, Selva A, Guazzi MD. Facilitation of coronary spasm by propranolol in Prinzmetal's angina: fact or unproven extrapolation? Coron Artery Dis. 1994;5:323–30.
9. Wallace A, Layug B, Tateo I, Li J, Hollenberg M, Browner W, Miller D, Mangano DT. Prophylactic atenolol reduces postoperative myocardial ischemia. McSPI Research Group. Anesthesiology. 1998;88:7–17.
10. Eguchi S, Kawano T, Yinhua, Tanaka K, Yasui S, Mawatari K, Takahashi A, Nakaya Y, Oshita S, Nakajo N. Effects of prostaglandin E_1 on vascular ATP-sensitive potassium channels. J Cardiovasc Pharmacol. 2007;50:686–91.
11. Endo M, Karasawa S, Kobayashi N, Nishida S. Coronary artery spasm during induced hypotensive anesthesia with prostaglandin E_1 (in Japanese with English abstract). Rinsho Masui (J Clin Anesth). 1994;18:667–8.
12. Furuya A, Matsukawa T, Kumazawa T. A case of coronary artery spasm during burr hole opening for craniotomy (in Japanese with English abstract). Masui (Jpn J Anesthesiol). 1996;45:1413–6.
13. Nagashima K, Miyata A, Kubota T, Maeda A, Ishinara H, Matsuki A. A case of coronary artery spasm during general anesthesia with continuous infusion of prostaglandin E_1 (in Japanese with English abstract). Rinsho Masui (J Clin Anesth). 1997;21:1309–10.
14. Kinoshita H, Matsuda N, Kimoto Y, Tohyama S, Hama K, Nakahata K, Hatano Y. Sevoflurane, but not propofol, prevents Rho kinase-dependent contraction induced by sphingosylphosphorylcholine in the porcine coronary artery. Anesth Analg. 2007;105:325–9.

Journal of Surgical Research xx, xxx (2008)
doi:10.1016/j.jss.2008.06.021

Exacerbation of Bleomycin-Induced Injury and Fibrosis by Pneumonectomy in the Residual Lung of Mice

Toru Kakizaki, M.D.,* Mitsutomo Kohno, M.D.,†,[1] Masazumi Watanabe, M.D.,† Atsushi Tajima, M.D.,† Yotaro Izumi, M.D.,† Taku Miyasho, V.M.D.,§ Sadatomo Tasaka, M.D.,‡ Koichi Fukunaga, M.D.,‡ Ikuro Maruyama, M.D.,¶ Akitoshi Ishizaka, M.D.,‡ and Koichi Kobayashi, M.D.†

*Department of Surgery, National Hospital Organization Kanagawa Hospital, Kanagawa, Japan; †Department of Surgery; and ‡Department of Medicine, Keio University School of Medicine, Tokyo, Japan; §Department of Veterinary Biochemistry, Rakuno Gakuen University, Hokkaido, Japan; ¶Department of Laboratory and Molecular Medicine, Faculty of Medicine, Kagoshima University, Kagoshima, Japan

Submitted for publication May 12, 2008

Background. **Lung resection after induction chemotherapy and/or radiotherapy for down-staging of locally advanced lung cancer can be complicated with lethal interstitial pneumonia. We studied the effects of pneumonectomy on bleomycin-induced lung injury and fibrosis in mice.**

Methods. **The mice underwent left pneumonectomy or a sham thoracotomy after intratracheal administration of saline or bleomycin. Lung permeability index, wet-to-dry weight ratio, histological changes, collagen contents, and concentrations of inflammatory mediators and cell counts in broncho-alveolar lavage (BAL) fluid were assessed in the residual right lung 7 d after surgery.**

Results. **The index of capillary permeability, lung water content, and inflammatory cell counts in BAL fluid were significantly increased by pneumonectomy. These measurements were highest in the mice with both pneumonectomy and intratracheal administration of bleomycin. Similarly, fibrotic change in lung pathology, as well as an increase in lung collagen content, was most prominent in the mice exposed to both interventions. The BAL fluid concentrations of interleukin-1β, interleukin-6, RANTES, and high mobility group box 1 were significantly increased by pneumonectomy and enhanced by the additional administration of bleomycin.**

Conclusions. **The results of this study indicate that pneumonectomy alone causes noncritical lung injury, which amplifies the inflammatory response to bleomycin and promotes lung fibrosis. Several inflammatory mediators appear to be involved in the exacerbation of bleomycin-induced lung injury and fibrosis.**

Key Words: **lung cancer; induction therapy; lung resection; acute lung injury/acute respiratory distress syndrome (ALI/ARDS); high mobility group box 1; bleomycin.**

INTRODUCTION

Lung cancer remains a highly lethal disease in many countries [1, 2]. Surgery offers the best chance for cure in patients with non-small cell lung cancer (NSCLC) at early stages [3]. However, only a few patients who have NSCLC with mediastinal lymph-node involvement (stage IIIA) are primary candidates for surgery alone. Induction chemotherapy alone or in association with radiotherapy has been applied to downstage the tumors and improve both surgical resectability and long-term survival for NSCLC at stage IIIA [4, 5]. Although there seems to be a general agreement that this strategy contributes to improve outcome at this advanced stage, the risks of complications in patients undergoing lung resection after induction therapy remain controversial [6, 7]. Some studies reported that the risk of postoperative complications and mortality is higher after induction therapy [7–9], whereas others observed a short-term outcome comparable with that of patients receiving surgery alone [6, 10]. The major causes of death reported most frequently are acute lung injury/acute respiratory distress syndrome (ALI/ARDS), pneumonia, bronchopleural fistula, and empyema. Analyzing the

[1] To whom correspondence and reprint requests should be addressed at Department of Surgery, Keio University School of Medicine, 35 Shinanomachi, Shinjuku-ku, Tokyo, 160-8582, Japan. E-mail: kohno@1993.jukuin.keio.ac.jp.

0022-4804/08 $36.00

literature, both postoperative morbidity and mortality are higher after pneumonectomy (PNX) than after lobectomy [9–12].

The increased rate of postoperative respiratory complications in patients having undergone induction therapy may be related to noninfectious diffuse lung damage caused by induction chemotherapy and/or radiotherapy [13, 14]. Radiotherapy-induced pulmonary toxicity with impairment of diffusion capacity has been reported [7, 15, 16] as well as that induced by chemotherapeutic agents, including bleomycin [17], mitomycin-C [18], gemcitabine [19], and cisplatin [19, 20]. Reduction in lung diffusion capacity after induction therapy is often subclinical but could expose patients to a greater risk of lung injury after surgery. The mechanisms underlying these modifications are still unclear.

Bleomycin (BLM) is an anti-cancer drug that causes diffuse alveolar injury and subsequent pulmonary fibrosis [21, 22]. Other investigators have observed that (1) proinflammatory cytokines, such as tumor necrosis factor (TNF)-α, interleukin (IL)-1β, and IL-6, (2) C-C chemokines, including monocyte chemoattractant protein (MCP)-1/CCL2, regulated on activation normal T cell expressed and secreted (RANTES)/CCL5 and macrophage inflammatory protein (MIP)-1α/CCL3, and (3) C-X-C chemokine keratinocyte-derived chemokine (KC)/CXCL1, are involved in BLM-induced lung inflammation and subsequent fibrotic process, including the promotion of fibroblast proliferation and collagen production [23–28]. In the present study, we administered a low dose of BLM to the mouse lung as a model of noninfectious diffuse lung damage followed by lung resection.

High mobility group box 1 (HMGB1) protein, originally identified as a non-histone, chromatin-associated protein, is also believed to possess proinflammatory properties [29]. Exposure of neutrophils or macrophages to HMGB1 induces nuclear translocation of nuclear factor-kappa B (NF-κB) and the enhanced production of proinflammatory cytokines, including TNF-α and IL-1β [30, 31]. Other investigators have found HMGB1 to be an important late mediator of endotoxin shock, and of various types of ALI [31–33]. Suda *et al.* have also suggested that HMGB1 participates in the pathogenesis of postoperative organ system dysfunction after exposure to a major surgical stress [34]. To the best of our knowledge, the role of HMGB1 in the inflammatory changes after pulmonary resection has not been examined.

We studied here the effects of PNX on the development of inflammatory responses and pulmonary fibrosis induced by BLM in mice. The concentrations of TNF-α, IL-1β, IL-6, MCP-1, MIP-1α, RANTES, KC, and HMGB1 were measured in broncho-alveolar lavage (BAL) fluid from the residual lung after PNX, exposure to BLM, or both.

METHODS

Animal Preparations

Specific, pathogen-free, 8-wk-old, inbred, male C57BL/6 mice, weighing 20–22 g, were purchased from CLEA Japan, Inc. (Tokyo, Japan). The mice were kept in a 12-h light/12-h dark cycle with free access to food and water. All mice received humane care, in compliance with Guiding Principles in the Care and Use of Animals adopted by the American Physiological Society. Experiments were conducted in accordance with protocols approved by our Institutional Review Board for animal studies. The mice were randomly assigned to one of four experimental groups: (1) intratracheal saline administration followed by thoracotomy (control group), (2) intratracheal administration of low dose BLM followed by thoracotomy (BLM group), (3) intratracheal saline administration followed by left PNX (PNX group), and (4) intratracheal administration of low dose BLM followed by left PNX (BLM + PNX group).

Experimental Model

The mice were anesthetized with 100 mg/kg of ketamine and 10 mg/kg of xylazine administered subcutaneously. They were intubated with an 18-gauge catheter and connected to a rodent ventilator, adjusted to maintain a respiratory rate of 100 breaths/min, 10-mL/kg tidal volume, 2-cm H_2O positive end-expiratory pressure, and 0.21 FiO_2. In the control group, 40 μL of saline was instilled into the right lung through the intratracheal tube, followed by sham operation. In the BLM group, 1.0 mg/kg of bleomycin hydrochloride (Nippon Kayaku, Tokyo, Japan) suspended in 40 μL of saline was instilled slowly into the right lung through the intratracheal tube, followed by sham operation. In the PNX group, 40 μL of saline was instilled into the right lung, followed by left PNX. In the BLM + PNX group, 1.0 mg/kg of bleomycin hydrochloride suspended in 40 μL of saline was instilled into the right lung, followed by left PNX. After intratracheal administration of saline or BLM, intratracheal tube was connected to the ventilator again. The chest was opened in all experimental groups after waiting for the respiratory movement to get stable for a few min. The left lungs were resected in the PNX and BLM + PNX groups. The chest was closed so that the open chest time was 5 min in all groups. And then the intratracheal tube was disconnected from the ventilator. Total duration of mechanical ventilation for the whole surgical procedure was fixed at 10 min.

Surgical Procedures

A 20-mm-long posterolateral skin incision was made, followed by thoracotomy in the fifth intercostal space with dissection of the serratus anterior and a latissimus dorsi muscles. In the sham operation groups, thoracotomy was closed without lung resection. In the PNX and BLM + PNX groups, the whole left lung was resected from the pleural cavity. The left main bronchus with left pulmonary artery and vein were ligated at the hilum with 5-0 silk before removal of the lung. The tidal volume was reduced from 10 to 6 mL/kg after the lung was removed. The fifth intercostal space was closed with a single surgical suture, and the skin and muscle incisions were closed with two sutures to avoid excessive tension on the muscles. The duration of mechanical ventilation for the whole surgical procedure was fixed at 10 min. All mice recovered quickly after extubation and were maintained for 7 d, before being euthanized by injection of 100 mg/kg of ketamine and 10 mg/kg of xylazine, followed by exsanguination from the inferior vena cava. The lungs were resected, and the blood was allowed to drain.

Bronchoalveolar Lavage Fluid

BAL was performed on the right lobes. The lungs were lavaged twice with 0.5 mL of saline. The fluid recovery always exceeded 90%, with no significant difference among groups. The BAL fluid was

centrifuged at 3000 rpm for 15 min, and the supernatant was stored at −80°C until later analyses. After centrifugation of the BAL fluid, the cell pellet was resuspended in 1 mL of saline, and the cells were counted by hemacytometry (Unopet Microcollection System; Becton Dickinson, Rutherford, NJ). The BAL cell smear was stained with a modified Wright's staining system (Diff-Quick; American Scientific Products, McGaw Park, IL), and 200 cells were randomly identified for differential cell counts.

Measurements

Lung Wet-to-Dry Weight Ratio

The lung wet-to-dry weight (W/D) ratio was measured to study the impact of left PNX on the formation of edema in the right lung. After their wet weight was measured, the right lower lobes were completely dried in a vacuum drying oven (DP22; Yamato Scientific, Tokyo, Japan) at 95°C and −270 cm H_2O for 48 h, to remove all gravimetrically detectable water. The pulmonary water accumulation was calculated as the W/D ratio.

Permeability Index

The permeability index, an index of alveolar epithelial and endothelial permeability, was calculated as the ratio of the concentration of human serum albumin (Buminate; Baxter Healthcare Corporation, Glendale, CA), which was intravenously injected 1 h before euthanasia, in BAL fluid to that in plasma.

Histological Examination

For histopathological examinations, the remaining lungs were inflated with 10% buffered formalin at a pressure of 10 cm H_2O. The lung tissue was embedded in paraffin and cut in 4-μm sections. The sections, stained with hematoxylin and eosin or Masson's trichrome, were prepared by standard techniques. The Ashcroft scale was used for the quantitative analysis of fibrotic changes induced by BLM [35]. Briefly, the grade of lung fibrosis was scored on a scale from 0 to 8 by examining 10 randomly chosen fields per sample, at a magnification of 100× by the same investigator, unaware of the experimental protocol. The grades of lung fibrosis were assigned as follows: grade 0, normal lung; grade 1, = minimal fibrous thickening of alveolar or bronchiolar walls; grade 3, moderate thickening of walls without obvious changes in the lung architecture; grade 5, increased fibrosis with definite changes in the lung structure and formation of fibrous bands or small fibrous masses; grade 7, severe distortion of structure and large fibrous areas; and grade 8, total fibrous obliteration of the fields.

Collagen Assay

The total collagen content of the right lung was determined by measuring the total soluble collagen, using the Sircol Collagen Assay kit (Biocolor, Belfast, Northern Ireland) according to the manufacturer's instructions. Briefly, the lungs were homogenized in 3 mL of 0.5 M acetic acid containing 1 mg of pepsin per 10 mg of tissue residue. Each sample was incubated and stirred for 24 h. After centrifugation, 100 μL of each supernatant was assayed. Then, 1 mL of Sircol dye reagent that specifically binds to collagen was added to each sample and mixed for 30 min. After centrifugation, the pellet was suspended in 1 mL of alkali reagent (0.5 M NaOH) included in the kit, and the absorbance measured at 540 nm with a spectrophotometer. The values in the test samples were compared with the values obtained with standard collagen solutions provided by the manufacturer and used to construct a standard curve.

HMGB1 and Cytokine Measurements

Enzyme-linked immunosorbent assay (ELISA) was performed to assess the HMGB1 concentrations in plasma and BAL fluid, using monoclonal antibodies to HMGB1 (Shino-Test. Co, Tokyo, Japan) [36]. To examine the cytokine profiles in BAL fluid, we used a suspension array technique (Bio-Plex; Bio-Rad Laboratories, Hercules, CA) for simultaneous measurements of IL-1β, IL-6, KC, MCP-1, MIP-1α, RANTES, and TNF-α.

Statistical Analysis

The statistical analyses were performed with the StatView-J 5.0 (Abacus Concepts Inc., Berkeley, CA) and Instat 3 (GraphPad Software Inc., San Diego, CA) software. Data are expressed as means ± standard error. Comparisons of histological scores were examined by Kruskal-Wallis nonparametric analysis of variance for factorial experiments, followed by Dunn's procedure for post hoc multiple comparisons analysis. The other data were analyzed by one-way analysis of variance followed by Scheffe's post hoc test for multiple comparisons. A P value <0.05 was considered statistically significant.

RESULTS

Increase in Lung W/D Ratio After Pneumonectomy and Bleomycin Administration

There was a significant difference in the mean lung W/D ratio between the control group and the other three study groups (control *versus* BLM, $P < 0.005$; control *versus* PNX, $P < 0.05$; control *versus* BLM + PNX, $P < 0.0001$). However, there was no significant difference in W/D ratio between the BLM and the PNX group. There was also a significant increase in the W/D ratio in the BLM + PNX group compared with the BLM and the PNX groups ($P < 0.01$ and $P < 0.001$, respectively; Fig. 1A).

Increase in Permeability Index After Pneumonectomy, and After Pneumonectomy Plus Bleomycin Administration

Whereas there was no significant difference in permeability index between the control and the BLM groups ($P = 0.35$), the increase in permeability index in the PNX group compared with control group was significant ($P < 0.05$), with an even greater difference between the control and the BLM + PNX groups ($P < 0.0001$). The increases in permeability index in the BLM + PNX group compared with the BLM group ($P < 0.0005$) and with the PNX group ($P < 0.005$) were also significant (Fig. 1B).

Increase in Inflammatory Cell Accumulations After Pneumonectomy and Bleomycin Administration

The total cell counts in BAL fluid increased significantly in the BLM, PNX, and BLM + PNX groups compared with the control group (control *versus* BLM, $P < 0.001$; control *versus* PNX, $P < 0.005$; control *versus* BLM + PNX, $P < 0.0001$). In the BLM group, neutrophils and macrophages were increased significantly (both $P < 0.05$) compared with the control

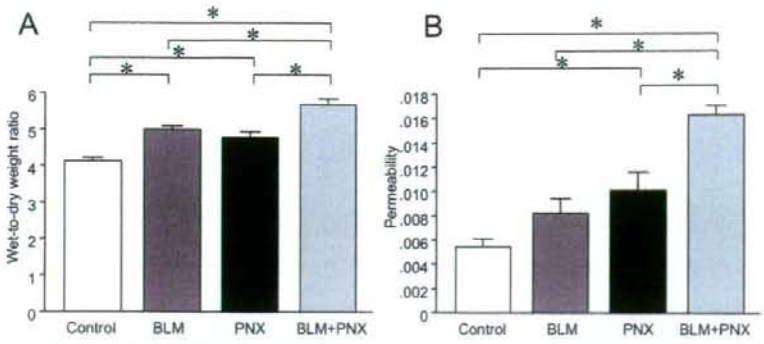

FIG. 1. Lung wet-to-dry (W/D) weight ratio (A) and permeability indices (B) assessed in the right lung of mice from the control, bleomycin (BLM), pneumonectomy (PNX), and BLM + PNX groups 7 d after the intratracheal instillation of BLM and/or left PNX. Values are means ± SE; $n = 8$ in each group. *, $P < 0.05$.

group. In the BLM + PNX group, neutrophils ($P < 0.0001$), lymphocytes ($P < 0.01$), macrophages ($P < 0.0001$), and total cell counts ($P < 0.0001$) were all increased significantly compared with the control group. Similarly significant increases were observed between the BLM + PNX and the PNX alone groups (neutrophils, $P < 0.0001$; lymphocytes, $P < 0.05$; macrophages, $P < 0.005$; total cells, $P < 0.0001$). The increases in the number of neutrophils ($P < 0.0001$) and total cells ($P < 0.0001$) in the BLM + PNX compared with the BLM group were also significant (Fig. 2).

Enhanced Fibrosis After Pneumonectomy Plus Bleomycin Administration

The histopathology of the right lung stained with hematoxylin and eosin and with Masson's trichrome in the four experimental groups is illustrated in Fig. 3. Slight septal thickening and infiltration of inflammatory cells was present in the PNX group (Fig. 3C). Alveolar septal thickening, characterized by interstitial infiltration with inflammatory cells and fibroblasts, were apparent in the BLM group (Fig. 3B). Collagen deposition was also detected by Masson's trichrome staining in the BLM group. However, fibrosis with distortion of normal lung architecture and enlargement of alveolar spaces was most prominent in the BLM + PNX group (Fig. 3D). The accumulation of inflammatory cells was also greatest in the BLM + PNX group. In the lungs stained with Masson's trichrome, an increased collagen deposition was distinct in the fibrotic region. There was a significant difference in the lung fibrosis scores between the control group and other three groups (control *versus* BLM, $P < 0.001$; control *versus* PNX, $P < 0.01$; control *versus* BLM + PNX, $P < 0.001$). The BLM + PNX group also revealed a significant increase in the Ashcroft fibrosis score compared with the BLM group ($P < 0.01$) and the PNX group ($P < 0.001$; Fig. 4).

Increase in Lung Collagen Content After Pneumonectomy Plus Bleomycin Administration

Pulmonary fibrosis was further assessed by measuring the collagen content in the right lung 7 d after BLM administration and PNX (Fig. 5). The collagen content was significantly increased in the BLM + PNX group compared with the control group (108 ± 25 *versus* 15 ± 4 ng/mg of tissue, $P < 0.001$). There was no other significant difference between the groups. The collagen contents in the lung tissues of the BLM and the PNX groups were 56 ± 7 and 54 ± 8 ng/mg, respectively, which were intermediate between those measured in the control and the BLM + PNX groups.

Elevated HMGB1 Level in BAL Fluid After Pneumonectomy

HMGB1 levels in the BAL fluid were significantly increased ($P < 0.01$ and $P < 0.001$, respectively) in the PNX group (64 ± 6 ng/mL) and the BLM + PNX group

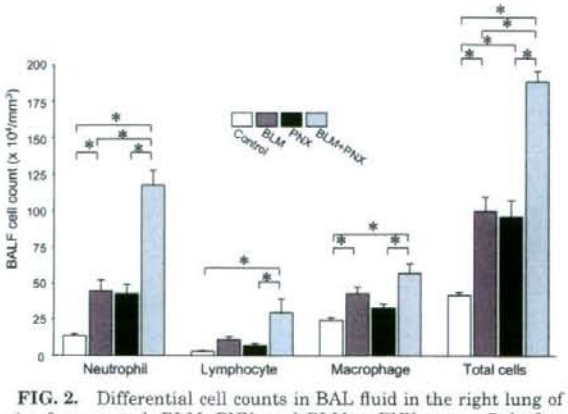

FIG. 2. Differential cell counts in BAL fluid in the right lung of mice from control, BLM, PNX, and BLM + PNX groups 7 d after intratracheal instillation of BLM and/or left PNX. Values are means ± SE; $n = 8$ in each group. *, $P < 0.05$.

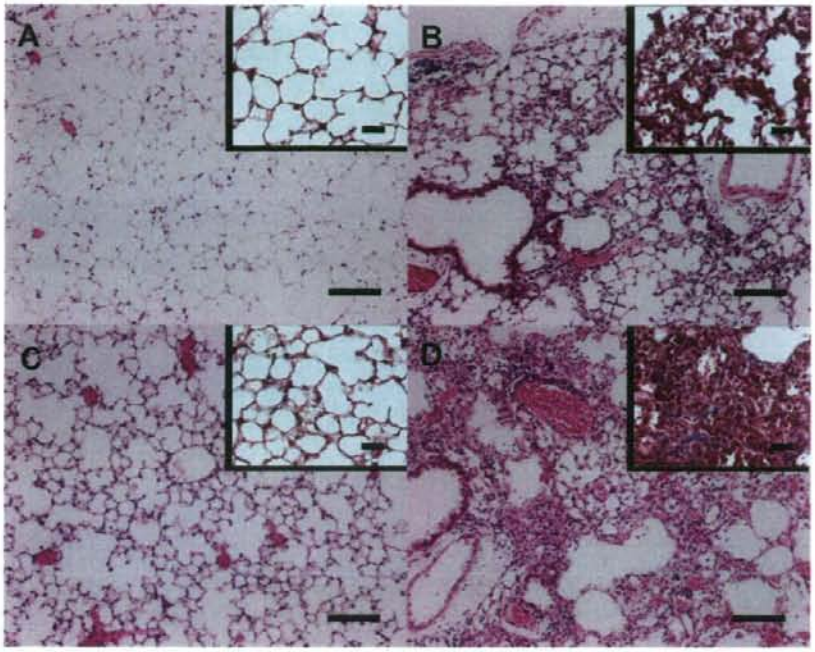

FIG. 3. Representative histological appearances of the right lung of mice from the control (A), BLM (B), PNX (C), and BLM + PNX (D) groups 7 d after intratracheal instillation of BLM and/or left PNX. The lung sections were stained with hematoxylin and eosin (H-E) to evaluate injury and fibrosis, and with Masson's trichrome to detect the deposition of collagen (insets). Prominent fibrotic changes with collagen deposition were observed in the BLM + PNX group (D), while similar, though less marked fibrotic changes are present in the BLM group (B). The H-E staining shows infiltration of inflammatory cells in the BLM (B) and PNX (C) groups. The BLM + PNX group had more prominent infiltration of inflammatory cells (D). Bars = 100 μm (outside the inset) or 50 μm (insets).

(72 ± 8 ng/mL), compared with the control group (26 ± 2 ng/mL). Furthermore, the difference in HMGB1 concentration in BAL fluid was also significant between the BLM (45 ± 6 ng/mL) and the BLM + PNX groups ($P < 0.05$; Fig. 6).

Increased Cytokine and Chemokine Concentrations in BAL Fluid After Pneumonectomy or Bleomycin Administration

The concentrations of TNF-α, IL-1β, IL-6, MCP-1, RANTES, MIP-1α, and C-X-C chemokine KC in the BAL fluid were measured 7 d after instillation of BLM, or PNX, or both (Fig. 7). The concentrations of IL-1β, IL-6, and RANTES increased significantly after the instillation of BLM only ($P < 0.05$, $P < 0.05$ and $P < 0.0005$, respectively) and after PNX only ($P < 0.005$, $P < 0.05$, $P < 0.001$, respectively) compared with the control group. In the BLM + PNX group, the concentrations of IL-1β, IL-6, KC, MCP-1, RANTES, and MIP-1α increased significantly compared with the control group ($P < 0.0001$, $P < 0.0001$, $P < 0.0001$, $P < 0.0001$, $P < 0.0001$, and $P < 0.005$, respectively). There was also a significant difference in the BAL fluid concentrations of IL-1β, IL-6, KC, MCP-1, and RANTES between the BLM and the BLM + PNX groups ($P < 0.05$, $P < 0.0001$, $P < 0.0005$, $P < 0.005$, and $P < 0.0001$, respectively), and a significant increase in IL-6, KC, MCP-1, and RANTES between the PNX and the BLM + PNX groups ($P < 0.0001$, $P < 0.0001$, $P < 0.0005$, and $P < 0.0001$, respectively). There were no significant differences in TNF-α concentrations in BAL fluid among the study groups on day 7.

DISCUSSION

The impact of PNX on noninfectious diffuse lung injury induced by BLM was determined in the present study. We found that PNX alone causes noncritical lung injury, which enhances the inflammatory response to BLM, and promotes subsequent fibrosis associated with the local up-regulation of several inflammatory mediators, such as HMGB1, IL-1β, IL-6, and RANTES. BLM is seldom used against NSCLC; however, it is reported that other cytotoxic agents such as cisplatin, which is frequently used for induction therapy, also cause diffuse lung damage [19, 20]. Our results suggest that similar mechanisms may underlie postoperative lung injury in patients with induction chemotherapy. The impact of pneumonectomy on lung

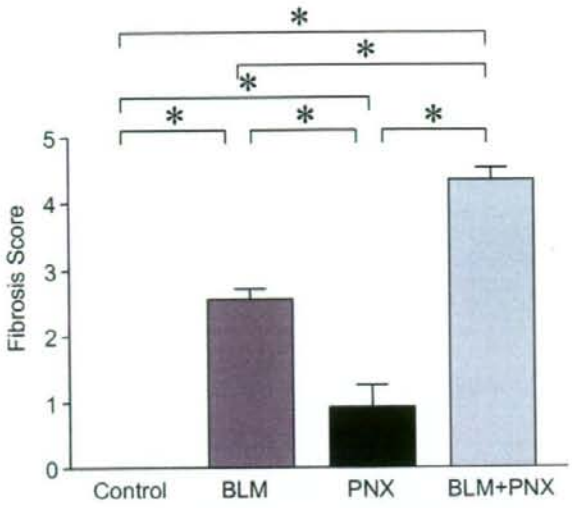

FIG. 4. The extent of fibrosis was assessed with Ashcroft score. The right lung of mice from the control, BLM, PNX, and BLM + PNX groups were examined 7 d after the intratracheal instillation of BLM and/or left PNX. The results are means ± SE; $n = 4$ in each group. *, $P < 0.05$.

inflammatory changes induced by cisplatin and/or gemcitabine, which are widely used for the treatment of lung cancer, should be investigated in future studies.

In the preliminary study, we have confirmed that pneumonectomized mice recovered quickly after surgery and survived more than several mo when they were not exposed to BLM. However, in the present work, pulmonary vascular hyperpermeability and lung water accumulation with inflammatory cell accumulation and cytokine up-regulation developed in the residual lung 7 d after PNX alone. This occult injury in the residual lung might not influence the outcome unless other predisposing factor exists. We found that the BLM-induced lung injury was exacerbated by PNX, manifest by an increased vascular permeability, W/D ratio, and leukocyte accumulation and by histological changes in the remaining lung.

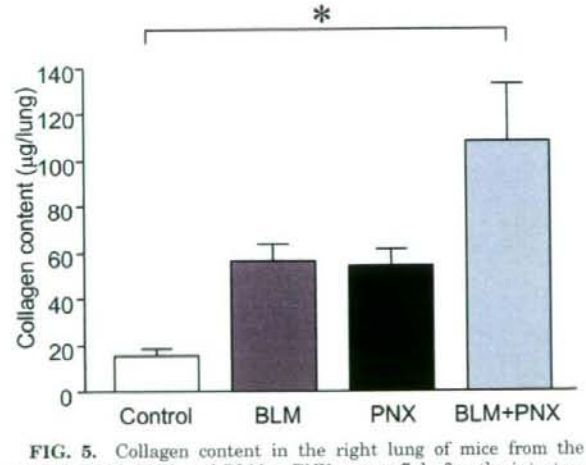

FIG. 5. Collagen content in the right lung of mice from the control, BLM, PNX, and BLM + PNX groups 7 d after the intratracheal instillation of BLM and/or left PNX. Values are means ± SE; $n = 8$ in each group. *, $P < 0.05$.

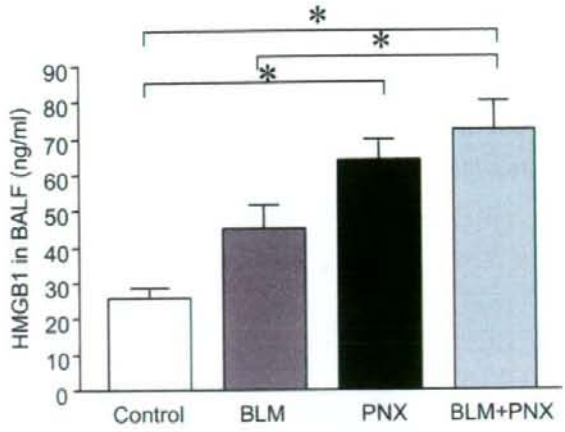

FIG. 6. High mobility group box 1 protein (HMGB1) concentration in BAL fluid in the right lung of mice from the control, BLM, PNX, and BLM + PNX groups, 7 d after the intratracheal instillation of BLM and/or left PNX. Values are means ± SE; $n = 8$ in each group. *, $P < 0.05$.

The dose of BLM administered into the lung was less than one-third the amount which has been used in previous studies of BLM-induced lung injury and fibrosis [37]. This was dictated by our preliminary experiments, in which no mouse in the BLM + PNX group survived for 7 d after having received the amount of BLM described in previous reports. Therefore, we reduced the dose of BLM so that the mice survived for at least 7 d after PNX and BLM instillation. This might explain the lack of a significant increase in permeability index or lung collagen content 7 d after BLM instillation alone, compared with the control group. However, this low dose of BLM caused a significant increase in the permeability index when combined with PNX. Moreover, the fibrotic response to BLM was enhanced by PNX, expressed by an increased lung content of soluble collagen and higher histological score in the BLM + PNX group.

BLM-induced lung injury has been used in studies of pulmonary fibrosis in animal models. In response to BLM, mice develop acute alveolitis and interstitial inflammation, characterized by the sequential recruitment of neutrophils, lymphocytes, and macrophages in the first wk. Following this inflammatory response, fibroblast proliferation and synthesis of extracellular matrix occur in the second wk [23, 26]. In the context of

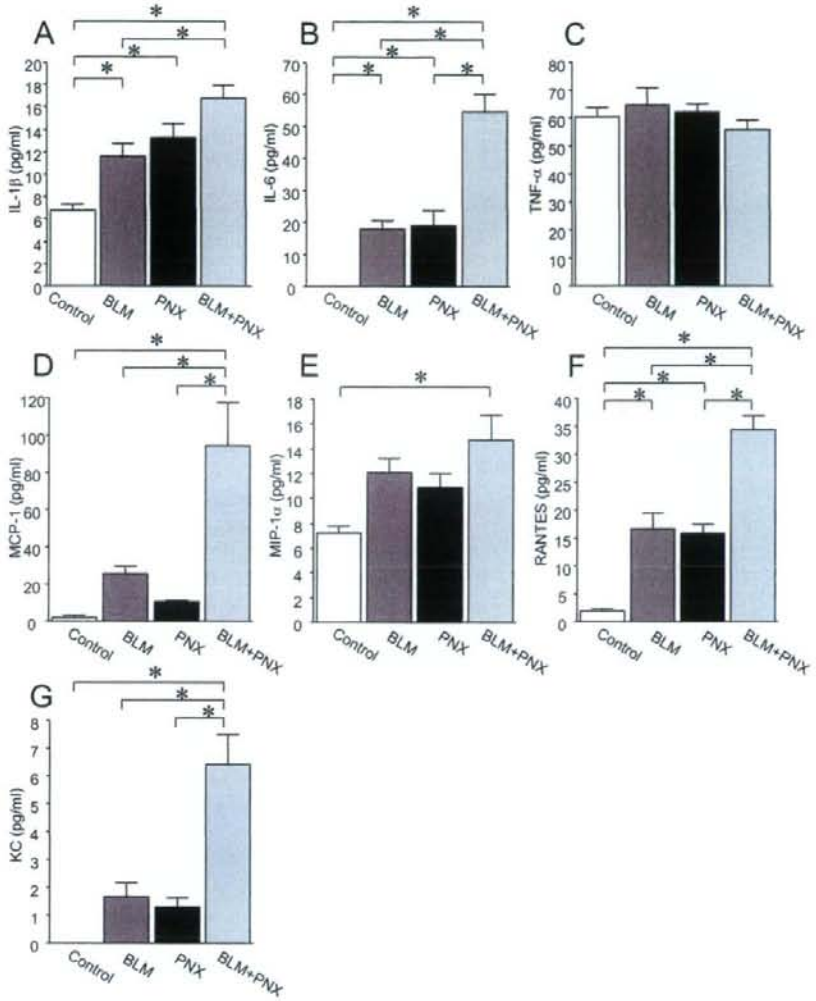

FIG. 7. Concentrations of IL-1β (A), IL-6 (B), TNF-α (C), MCP-1 (D), MIP-1α (E), RANTES (F), KC (G) measured in BAL fluid in the right lung of mice from the control, BLM, PNX, and BLM + PNX groups, 7 d after the intratracheal instillation of BLM and/or left PNX. Values are means ± SE; $n = 8$ in each group. *, $P < 0.05$.

these pulmonary fibrotic changes, one might hypothesize that, in our model, the occult injury caused by PNX synergistically enhanced the BLM-induced inflammatory response in the residual lung in the first phase, and accelerated the subsequent proliferation of fibroblast and collagen deposition in interstitial tissue.

In clinical settings, BLM is never injected intratracheally, and a single dose of BLM administered systemically to human adults is limited to less than 0.5 mg/kg. However, since BLM accumulatively causes lung damages, intratracheal injection of 1 mg/kg BLM, which is adopted in our study, could be comparable to the repeated injection of smaller doses of BLM like in the real practice. Therefore, we think that our model is applicable to elucidate the pathogenesis of human lung injury and fibrosis caused by PNX and BLM.

Proinflammatory cytokines, such as TNF-α, IL-1β, and IL-6, are involved in the development of BLM-induced lung injury and fibrosis [23, 25, 38]. It has been suggested that TNF-α and IL-1β promote the proliferation of fibroblasts and their production of collagen, and that IL-6 stimulates the expression of MIP-1α in BLM-induced lung injury and fibrosis [23, 38, 39]. In the present study, PNX and BLM together increased the local concentration of IL-1β and IL-6 in the BLM, the PNX, and the BLM +PNX groups. How-

ever, neither BLM nor PNX made changes in TNF-α level on day 7, perhaps because TNF-α, an early-phase cytokine, peaks earlier than 7 d after PNX or BLM instillation.

The transmigration of inflammatory cells from the vascular space into the inflammatory sites is regulated mainly by various chemokines. The chemotactic activity of C-C chemokines, including MIP-1α, MCP-1, and RANTES, is mainly toward monocytes and lymphocytes, whereas the C-X-C chemokines, such as KC, attract neutrophils [40]. Several investigators have suggested that MIP-1α, RANTES, KC, and MCP-1 are involved in the accumulation of inflammatory leukocytes in lungs instilled with BLM and play important roles in the subsequent fibrotic process [24, 27, 28]. In our study, the concentration of RANTES in BAL fluid was significantly increased by either BLM or PNX, and the increase was greater when BLM was followed by PNX. Compared with their control values, MCP-1, MIP-1α, and KC increased significantly only when both interventions were combined. The up-regulation of MCP-1, MIP-1α, and KC was not induced by BLM alone, possibly because the dose of BLM instilled was lower than that in the previous investigations. PNX and BLM may synergistically up-regulate these chemokines and induce accumulation of inflammatory cells.

HMGB1 is an important determinant of mortality and organ system dysfunction in animal models of infection, such as bacterial peritonitis and endotoxin exposure, hemorrhagic shock, and ventilator-induced lung injury [32, 33, 41]. The intratracheal administration of HMGB1 is also known to cause ALI, and antibodies against HMGB1 attenuate the severity of endotoxin-induced pulmonary edema [29, 42]. In the present study, the sublethal lung injury that developed after PNX was associated with a significant increase in HMGB1 in BAL fluid. In addition, the HMGB1 concentrations in the BLM-challenged lungs were further increased by subsequent PNX. HMGB1 might be involved in the pathogenesis of post-PNX occult lung injury and in the exacerbation of BLM-induced lung injury by stimulating neutrophils or macrophages to enhance the production of proinflammatory cytokines, including IL-1β [30, 32, 33].

Ogawa *et al.* have suggested that overinflation of the lung might stimulate the release of HMGB1 in the model of ventilator-induced lung injury [41]. In our model, although we reduced the tidal volume after PNX, we observed prominent inflation of the right lung, protrusion of the diaphragmatic lobe into the left pleural cavity, and a left-shift of the mediastinum in the PNX group at the time of sacrifice, similar to that observed clinically in residual lungs after PNX [43]. Overinflation of the residual lung after PNX may cause lung tissue injury with release of HMGB1 into the alveolar space [41]. In addition, overinflation of the lung might widen the intercellular gaps between endothelial cells, epithelial cells, or both, allowing neutrophils to migrate into the alveolar space. HMGB1 in the lung may be released not only from injured cells, but also from greater numbers of activated neutrophils and macrophages [29].

Other investigators have observed that HMGB1 stimulates the secretion of several cytokines and chemokines, including IL-1β, TNF-α, IL-6, IL-8, MIP-1α, MCP-1, RANTES, from neutrophils, macrophages, or endothelial cells [32, 44, 45]. On the other hand, cytokines, including IL-1β, stimulate the secretion of HMGB1 by macrophages [29]. The combined activity of these inflammatory mediators might be responsible for the occult lung injury caused by PNX, and exacerbation of lung injury and fibrosis caused by BLM. Up-regulated mediators, such as IL-1β, IL-6, RANTES, and HMGB1, may be potential targets for preventing such lung injury and fibrosis after PNX.

In conclusion, we have shown that PNX exacerbated the injury and subsequent fibrosis induced by BLM in the residual lung. PNX alone caused lung injury with the local up-regulation of HMGB1 and of several cytokines and chemokines, such as IL-1β, IL-6, and RANTES. The enhanced release of these mediators might contribute to the exacerbation of the injury and fibrosis that developed in the residual lung exposed to BLM. Although our model does not closely approximate the clinical situation with respect to the drug administration, similar mechanisms may underlie ALI/ARDS after lung resection in patients with noninfectious diffuse lung damage, including those after induction chemotherapy and/or radiotherapy for locally advanced NSCLC.

ACKNOWLEDGMENTS

This study was supported in part by a Grant-in-Aid for Scientific Research (no. 18120101, 2006, for I. Maruyama and K. Kobayashi) from the Ministry of Education, Science, Sports and Culture.

REFERENCES

1. Jemal A, Siegel R, Ward E, et al. Cancer Statistics, 2008. CA Cancer J Clin 2008;58:71.
2. Watanabe S, Asamura H, Suzuki K, et al. Recent results of postoperative mortality for surgical resections in lung cancer. Ann Thorac Surg 2004;78:999; discussion 1002.
3. Wright G, Manser RL, Byrnes G, et al. Surgery for non-small cell lung cancer: Systematic review and meta-analysis of randomised controlled trials. Thorax 2006;61:597.
4. Rosell R, Gomez-Codina J, Camps C, et al. A randomized trial comparing preoperative chemotherapy plus surgery with surgery alone in patients with non-small-cell lung cancer. N Engl J Med 1994;330:153.
5. Roth JA, Fossella F, Komaki R, et al. A randomized trial comparing perioperative chemotherapy and surgery with surgery alone in resectable stage IIIA non-small-cell lung cancer. J Natl Cancer Inst 1994;86:673.

6. Mansour Z, Kochetkova EA, Ducrocq X, et al. Induction chemotherapy does not increase the operative risk of pneumonectomy! Eur J Cardiothorac Surg 2007;31:181.
7. Roberts JR, Eustis C, Devore R, et al. Induction chemotherapy increases perioperative complications in patients undergoing resection for non-small cell lung cancer. Ann Thorac Surg 2001; 72:885.
8. Depierre A, Milleron B, Moro-Sibilot D, et al. Preoperative chemotherapy followed by surgery compared with primary surgery in resectable stage I (except T1N0), II, and IIIa non-small-cell lung cancer. J Clin Oncol 2002;20:247.
9. Martin J, Ginsberg RJ, Abolhoda A, et al. Morbidity and mortality after neoadjuvant therapy for lung cancer: The risks of right pneumonectomy. Ann Thorac Surg 2001;72:1149.
10. Perrot E, Guibert B, Mulsant P, et al. Preoperative chemotherapy does not increase complications after nonsmall cell lung cancer resection. Ann Thorac Surg 2005;80:423.
11. Leo F, Solli P, Veronesi G, et al. Does chemotherapy increase the risk of respiratory complications after pneumonectomy? J Thorac Cardiovasc Surg 2006;132:519.
12. Venuta F, Anile M, Diso D, et al. Operative complications and early mortality after induction therapy for lung cancer. Eur J Cardiothorac Surg 2007;31:714.
13. Leo F, Solli P, Spaggiari L, et al. Respiratory function changes after chemotherapy: An additional risk for postoperative respiratory complications? Ann Thorac Surg 2004;77:260, discussion 265.
14. Takeda S, Funakoshi Y, Kadota Y, et al. Fall in diffusing capacity associated with induction therapy for lung cancer: A predictor of postoperative complication? Ann Thorac Surg 2006; 82:232.
15. Gopal R, Starkschall G, Tucker SL, et al. Effects of radiotherapy and chemotherapy on lung function in patients with non-small-cell lung cancer. Int J Radiat Oncol Biol Phys 2003;56: 114.
16. Miller KL, Zhou SM, Barrier RC Jr, et al. Long-term changes in pulmonary function tests after definitive radiotherapy for lung cancer. Int J Radiat Oncol Biol Phys 2003;56:611.
17. Horning SJ, Adhikari A, Rizk N, et al. Effect of treatment for Hodgkin's disease on pulmonary function: Results of a prospective study. J Clin Oncol 1994;12:297.
18. Castro M, Veeder MH, Mailliard JA, et al. A prospective study of pulmonary function in patients receiving mitomycin. Chest 1996;109:939.
19. Maas KW, van der Lee I, Bolt K, et al. Lung function changes and pulmonary complications in patients with stage III non-small cell lung cancer treated with gemcitabine/cisplatin as part of combined modality treatment. Lung Cancer 2003;41: 345.
20. Bhalla KS, Wilczynski SW, Abushamaa AM, et al. Pulmonary toxicity of induction chemotherapy prior to standard or high-dose chemotherapy with autologous hematopoietic support. Am J Respir Crit Care Med 2000;161:17.
21. Blum RH, Carter SK, Agre K. A clinical review of bleomycin–a new antineoplastic agent. Cancer 1973;31:903.
22. Rabinowits M, Souhami L, Gil RA, et al. Increased pulmonary toxicity with bleomycin and cisplatin chemotherapy combinations. Am J Clin Oncol 1990;13:132.
23. Smith RE, Strieter RM, Phan SH, et al. TNF and IL-6 mediate MIP-1alpha expression in bleomycin-induced lung injury. J Leukoc Biol 1998;64:528.
24. Smith RE, Strieter RM, Phan SH, et al. Production and function of murine macrophage inflammatory protein-1 alpha in bleomycin-induced lung injury. J Immunol 1994;153:4704.
25. Suwabe A, Takahashi K, Yasui S, et al. Bleomycin-stimulated hamster alveolar macrophages release interleukin-1. Am J Pathol 1988;132:512.
26. Tokuda A, Itakura M, Onai N, et al. Pivotal role of CCR1-positive leukocytes in bleomycin-induced lung fibrosis in mice. J Immunol 2000;164:2745.
27. Yara S, Kawakami K, Kudeken N, et al. FTS reduces bleomycin-induced cytokine and chemokine production and inhibits pulmonary fibrosis in mice. Clin Exp Immunol 2001; 124:77.
28. Zhang K, Gharaee-Kermani M, Jones ML, et al. Lung monocyte chemoattractant protein-1 gene expression in bleomycin-induced pulmonary fibrosis. J Immunol 1994;153:4733.
29. Wang H, Bloom O, Zhang M, et al. HMG-1 as a late mediator of endotoxin lethality in mice. Science 1999;285:248.
30. Park JS, Gamboni-Robertson F, He Q, et al. High mobility group box 1 protein interacts with multiple Toll-like receptors. Am J Physiol Cell Physiol 2006;290:C917.
31. Yamada S, Maruyama I. HMGB1, a novel inflammatory cytokine. Clin Chim Acta 2007;375:36.
32. Kim JY, Park JS, Strassheim D, et al. HMGB1 contributes to the development of acute lung injury after hemorrhage. Am J Physiol Lung Cell Mol Physiol 2005;288:L958.
33. Ueno H, Matsuda T, Hashimoto S, et al. Contributions of high mobility group box protein in experimental and clinical acute lung injury. Am J Respir Crit Care Med 2004;170:1310.
34. Suda K, Kitagawa Y, Ozawa S, et al. Serum concentrations of high-mobility group box chromosomal protein 1 before and after exposure to the surgical stress of thoracic esophagectomy: A predictor of clinical course after surgery? Dis Esophagus 2006; 19:5.
35. Ashcroft T, Simpson JM, Timbrell V. Simple method of estimating severity of pulmonary fibrosis on a numerical scale. J Clin Pathol 1988;41:467.
36. Yamada S, Inoue K, Yakabe K, et al. High mobility group protein 1 (HMGB1) quantified by ELISA with a monoclonal antibody that does not cross-react with HMGB2. Clin Chem 2003;49:1535.
37. Endo M, Oyadomari S, Terasaki Y, et al. Induction of arginase I and II in bleomycin-induced fibrosis of mouse lung. Am J Physiol Lung Cell Mol Physiol 2003;285:L313.
38. Saito F, Tasaka S, Inoue KI, et al. Role of interleukin-6 in bleomycin-induced lung inflammatory changes in mice. Am J Respir Cell Mol Biol 2008;38:566.
39. Karmiol S, Phan SH. Fibroblast and cytokines. In: Kunkel SL, Remick DG, Eds. Cytokines in Health and Disease. New York, NY: Dekker, 1992:271–296.
40. Oppenheim JJ, Zachariae CO, Mukaida N, et al. Properties of the novel proinflammatory supergene "intercrine" cytokine family. Annu Rev Immunol 1991;9:617.
41. Ogawa EN, Ishizaka A, Tasaka S, et al. Contribution of high-mobility group box-1 to the development of ventilator-induced lung injury. Am J Respir Crit Care Med 2006;174:400.
42. Abraham E, Arcaroli J, Carmody A, et al. HMG-1 as a mediator of acute lung inflammation. J Immunol 2000;165:2950.
43. Harada K, Hamaguchi N, Shimada Y, et al. Use of sulfur hexafluoride, SF6, in the management of the postpneumonectomy pleural space. Respiration 1984;46:201.
44. Andersson U, Wang H, Palmblad K, et al. High mobility group 1 protein (HMG-1) stimulates proinflammatory cytokine synthesis in human monocytes. J Exp Med 2000;192:565.
45. Fiuza C, Bustin M, Talwar S, et al. Inflammation-promoting activity of HMGB1 on human microvascular endothelial cells. Blood 2003;101:2652.

doi:10.1510/icvts.2007.170456

INTERACTIVE CARDIOVASCULAR AND THORACIC SURGERY

Interactive CardioVascular and Thoracic Surgery 7 (2008) 1114-1120

www.icvts.org

Negative results - Thoracic general

Occult injury in the residual lung after pneumonectomy in mice☆

Atsushi Tajima[a], Mitsutomo Kohno[b,*], Masazumi Watanabe[b], Yotaro Izumi[b], Sadatomo Tasaka[c], Ikuro Maruyama[d], Taku Miyasho[e], Koichi Kobayashi[b]

[a]Department of Surgery, Saiseikai Utsunomiya Hospital, Tochigi, Japan
[b]Department of Surgery, Keio University School of Medicine, 35 Shinanomachi, Shinjuku-ku, Tokyo, 160-8582, Japan
[c]Department of Medicine, Keio University School of Medicine, Tokyo, Japan
[d]Department of Laboratory and Molecular Medicine, Faculty of Medicine, Kagoshima University, Kagoshima, Japan
[e]Department of Veterinary Biochemistry, Rakuno Gakuen University, Hokkaido, Japan

Received 19 October 2007; received in revised form 20 May 2008; accepted 17 July 2008

Abstract

Objectives: We aimed to determine the acute phase impact of pneumonectomy with respect to injury in the remaining lung using a murine model, and to investigate the profiles of inflammatory mediators including high mobility group box 1 protein (HMGB1) following surgery and administration of low dose intratracheal lipopolysaccharide. **Methods:** Mice received left pneumonectomy with intratracheal administration of either saline or lipopolysaccharide. Lung permeability index, lung wet-to-dry weight ratio, pathological findings, HMGB1 levels in bronchoalveolar lavage fluid (BALF) and plasma, and cytokine profiles in BALF were assessed 24 h after surgery. **Results:** Index of capillary permeability, lung water content, and neutrophil and macrophage counts in BALF were significantly increased by pneumonectomy. These parameters were highest in the mice with pneumonectomy with intratracheal administration of lipopolysaccharide. On lung pathology, neutrophil infiltration was prominent in the residual lung after pneumonectomy. HMGB1 levels were significantly higher in both BALF and plasma in the mice with pneumonectomy, and were highest in those with pneumonectomy and intratracheal administration of lipopolysaccharide. Pro-inflammatory cytokine levels including interferon-γ significantly increased in BALF in the mice with pneumonectomy. **Conclusions:** It was suggested that pneumonectomy itself may cause occult lung injury in the acute phase (24 h) of post-surgery which could be enhanced by inflammatory stimulus, such as bacterial component, leading to significant lung injury. HMGB1 might be involved in the pathogenesis of the occult lung injury.

Keywords: Pneumonectomy; Lung injury; Endotoxin; HMGB1

1. Introduction

Lung cancer remains the leading cause of cancer death in Japan and many other developed countries [1]. Surgical resection, with or without adjuvant chemotherapy and radiotherapy, is currently the treatment of choice for early stage non-small cell lung cancer [2]. Although major advances in thoracic surgery have led to a significant reduction in postoperative complications following lung resection, it is always important for surgeons to try to reduce perioperative mortality [1, 3].

The major cause of morbidity and mortality following lung resection is respiratory complications. Acute lung injury (ALI), which develops in approximately 5% of patients undergoing lung resection, is responsible for the vast majority of respiratory-related deaths following thoracic surgery [4]. ALI following thoracotomy and lung resection has a grave prognosis, with overall hospital mortality rates over 20%. In some series limited to pneumonectomy, the mortality rates rose as high as 100% [5, 6]. The mortality rate of ALI following lung resection is higher than the mortality rate of ALI from all causes [7].

High mobility group box 1 protein (HMGB1), originally identified as a DNA binding protein, is an abundant and highly conserved cellular protein, which stabilizes nucleosome formation and facilitates gene transcription [8, 9]. HMGB1 also has potent pro-inflammatory properties [9, 10]. Exposure of neutrophils or macrophages to HMGB1 induces nuclear translocation of NF-κB and enhances production of pro-inflammatory cytokines, including tumor necrosis factor (TNF)-α and interleukin (IL)-1β, at least in part through the interaction of HMGB1 with Toll-like receptor (TLR)-2, TLR-4 and receptor for advanced glycation end products (RAGE) [11, 12]. Serum concentration of HMGB1 increased significantly 8–32 h after administration of lipopolysaccharide (LPS) or TNF-α in mice [10]. Intratracheal injection of HMGB1 results in the development of acute pulmonary inflammation, and blockade of HMGB1 decreases the severity of LPS-induced ALI, implicating HMGB1 as a mediator of sepsis-associated lung injury [9, 10]. Systemic administration of recombinant HMGB1 is lethal in mice [9, 10]. HMGB1 is also an important mediator of mortality and organ system dysfunction including ALI in animal models of conditions

☆ This study was partly supported by the Ministry of Education, Science, Sports and Culture, Grant-in-Aid for Scientific Research, 18120101, 2006, for I. Maruyama and K. Kobayashi.

*Corresponding author. Tel.: +81-3-5363-3806; fax: +81-3-5363-3499.
E-mail address: kohno@1993.jukuin.keio.ac.jp (M. Kohno).

such as bacterial peritonitis, lung transplantation, ventilator-induced lung injury and hemorrhage [13–18]. It has been suggested that HMGB1 contributes to the clinical course of ALI and postoperative complications [13, 19]. We therefore hypothesize that the postoperative HMGB1 level in plasma or organs may be useful as a parameter of surgical invasiveness and predictive of postoperative complication.

In this study, we aimed to determine the acute phase impact, meaning the impact of within 24 h, of pneumonectomy with respect to injury to the remaining lung in a murine model [20]. We administered a low dose of LPS to the residual lung as a model of ALI following lung resection. The profiles of inflammatory cytokines and HMGB1 were investigated to evaluate their roles in the pathogenesis of post-pneumonectomy lung injury.

2. Materials and methods

2.1. Experimental model

Specific pathogen-free inbred male C57BL/6 mice, eight-week-old and weighing 20–22 g were used. All experiments were conducted in accordance with protocols approved by the institutional review board for animal studies. Under general anesthesia, they were intubated with an 18-gauge intravenous catheter and connected to a rodent ventilator, which was adjusted to maintain normal ventilation (respiratory rate, 80 min; tidal volume, 10 ml/kg; positive end-expiratory pressure, 2 cm H_2O; FiO_2, 0.21). Mice were randomly assigned to one of four experimental groups. In the control group, 30 μl of saline was instilled into the lungs through the intratracheal tube. In the LPS group, 150 μg of LPS from *Escherichia coli* O55: B5 (Sigma, St Louis, MO) suspended in 30 μl of saline was instilled slowly into the lungs through the intratracheal tube, to create mild lung injury. In the pneumonectomy (PNX) group, 30 μl of saline was instilled into the lungs, followed by left pneumonectomy. In the LPS+PNX group, 150 μg of LPS diluted in 30 μl of saline was instilled into the lungs, followed by left pneumonectomy. The tidal volume was reduced from 10–6 ml/kg after the lung was removed. Human serum albumin (25 μg/100 μl; Buminate, Baxter Healthcare Corporation, Glendale, CA) was injected via tail vein 1 h before euthanasia to assess transvascular albumin leakage.

2.2. Parameters of lung injury

To investigate the impact of left pneumonectomy on the right lung, mice in the four groups were euthanized 24 h after surgery. The parameters to investigate lung injury were as follow: 1) lung wet-to-dry (W/D) weight ratio to estimate the severity of pulmonary edema; 2) ratio of human albumin concentrations in bronchoalveolar lavage fluid (BALF) to that in plasma (albumin B/P ratio) to assess transvascular albumin leakage (permeability index); 3) total and differential cell counts in BALF to assess inflammatory cell sequestration.

2.3. Histological examination

The degree of microscopic injury to the right lung was scored based on the following variables: hemorrhage, edema and neutrophil infiltration. The severity of injury was judged according to the following criteria: no injury=0; injury to 25% of the field=1; injury to 50% of the field=2; injury to 75% of the field=3, and diffuse injury=4 [21].

2.4. Micro-computed tomography

Lung images were obtained by a micro-computed tomography (CT) device, the LaTheta LCT-100A (ALOKA, Inc., Tokyo, Japan), to investigate the extent of lung infiltration 24 h after the intervention.

2.5. HMGB1 and cytokine measurements

ELISA was performed to detect HMGB1 levels in plasma and BALF using monoclonal antibodies to HMGB1 (Shino-Test. Co, Tokyo, Japan) [22]. To investigate cytokine profiles in BALF, we employed a Bio-Plex mouse cytokine assay (Bio-Rad Laboratories, Hercules, CA) for simultaneous quantitation of interleukin (IL)-1β, IL-6, IL-10, interferon (IFN)-γ, keratinocyte-derived chemokine (KC) and tumor necrosis factor (TNF)-α.

2.6. Statistical analysis

Comparisons of histological scores were examined by Kruskal–Wallis non-parametric analysis of variance for factorial experiments, followed by Dunn's procedure for post-hoc multicomparison analysis. Other results were analyzed by one-way ANOVA followed by a Scheffe's post-hoc test for multiple comparisons. Data are expressed as mean±S.D. A P-value of <0.05 was considered statistically significant.

3. Results

3.1. Lung W/D weight ratio was increased in the groups with pneumonectomy

There was a significant difference in the mean lung W/D weight ratio between the control group and the surgical groups (3.69 ± 0.07 vs. 4.92 ± 0.60, $P<0.001$, vs. 5.23 ± 0.25, $P<0.0001$), but there was no significant difference between the control group and the LPS group, between the LPS group and the PNX group, or between the PNX group and the LPS+PNX group. There was, however, a significant difference between the LPS group and the LPS+PNX group (4.26 ± 0.41 vs. 5.23 ± 0.25, $P<0.005$) (Fig. 1a).

3.2. Permeability index increased after pneumonectomy, and increased even more after pneumonectomy plus LPS administration

Although there was no significant difference in the permeability index between the control group and the LPS group (0.0034 ± 0.0006 vs. 0.0060 ± 0.0013, $P=0.64$), there was a significant difference in the permeability index between the control group and the PNX group ($0.0034\pm$

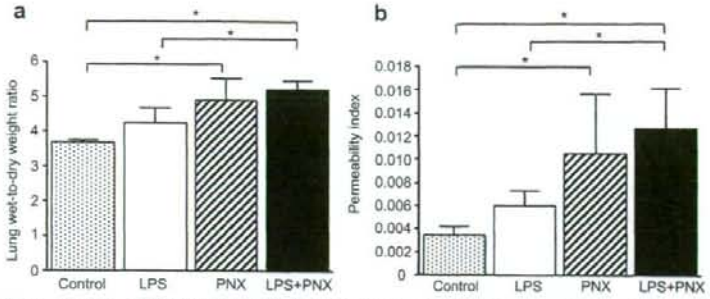

Fig. 1. (a) Lung wet-to-dry (W/D) weight ratio. (b) Permeability index: Ratio of albumin concentration in bronchoalveolar lavage fluid to that in plasma (albumin B/P ratio). There were significant differences in the lung W/D ratio and permeability index between the control group and the two groups with pneumonectomy. Values are means±S.D.; $n=6$. *$P<0.05$. Scheffe's post-hoc test.

0.0006 vs. 0.0105±0.0051, $P<0.05$) and between the control group and the LPS+PNX group (0.0034±0.0006 vs. 0.0127±0.0034, $P<0.01$). There was also a significant increase in the permeability index in the LPS+PNX group compared with the LPS group (0.0060±0.0013 vs. 0.0127±0.0034, $P<0.05$) (Fig. 1b).

3.3. Different cell accumulations in the pneumonectomy groups

The total cell counts in BALF increased significantly in all three experimental groups compared to the control group. The cell patterns differed between the groups. In the LPS group, only neutrophils were increased significantly. In the PNX group, neutrophils, lymphocytes and macrophages were all increased significantly (Fig. 2).

3.4. Lung histology: significant neutrophil infiltrations

Pneumonectomy alone induced significant neutrophil infiltration, although there was no significant difference in scores for hemorrhage and edema between the control and PNX groups. Instillation of LPS induced significant neutrophil infiltration with hemorrhage and edema of the lung. The severity of damage was significantly greater following pneumonectomy plus instillation of LPS than the other groups (Figs. 3 and 4).

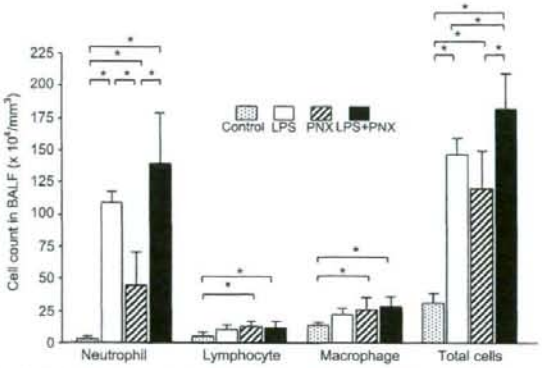

Fig. 2. Cell counts in bronchoalveolar lavage fluid. Neutrophils, lymphocytes and macrophages were all increased significantly in the PNX group compared with the control group. In the LPS group, only neutrophils increased significantly, compared with the control group. Values are means±S.D.; $n=6$. *$P<0.05$. Scheffe's post-hoc test.

3.5. Micro-computed tomography: severe damage to the lungs of the LPS+PNX group

CT for small animals following left pneumonectomy showed extensive inflation of the right lung, protrusion of the diaphragmatic lobe into the left pleural cavity, and left-shifted mediastinum. Infiltration was observed in the

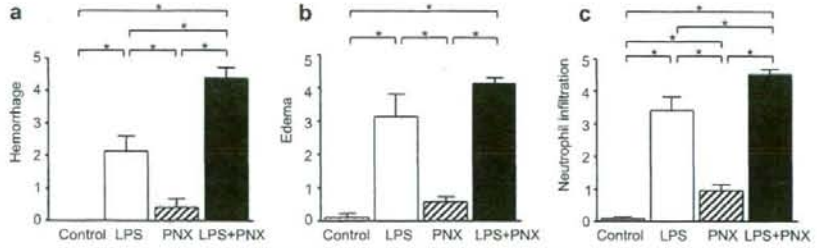

Fig. 3. The degree of microscopic injury was scored based on the following variables: hemorrhage (a), edema (b) and neutrophil infiltration (c). The severity of injury was judged according to the following criteria: no injury=0; injury to 25% of the field=1; injury to 50% of the field=2; injury to 75% of the field=3 and diffuse injury=4. Values are means±S.D.; $n=6$. *$P<0.05$. Dunn's multiple post-hoc test.

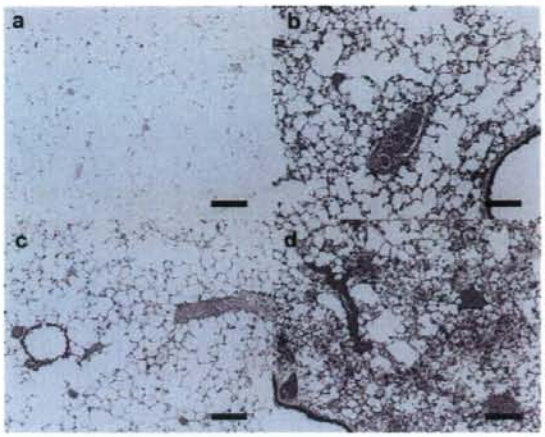

Fig. 4. Histopathological findings in the right lung of mice from the control group (a), the LPS group (b), the PNX group (c), and the LPS+PNX group (d). Remarkable cell infiltration is visible in the LPS group (b), and a similar but milder change is observed in the PNX group (c). The most severe damage is seen in the LPS+PNX group (d). Bars = 100 μm.

right lungs of the groups with LPS instillation. The infiltration area was more extensive in the LPS+PNX group than in the LPS group (Fig. 5).

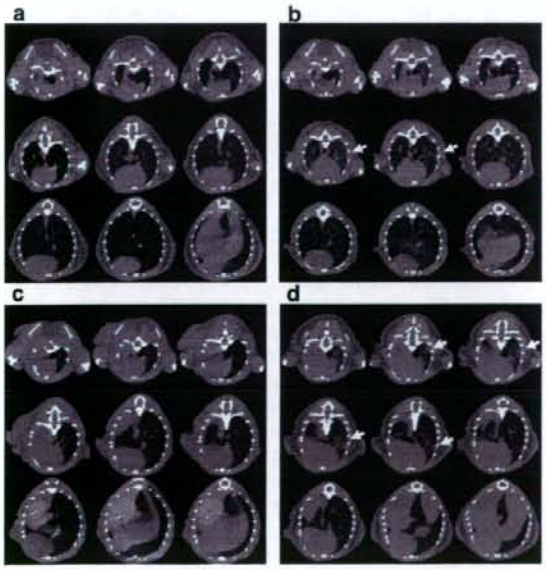

Fig. 5. Representative findings of the micro-computed tomography to evaluate the extent of lung infiltration from the control group (a), the LPS group (b), the PNX group (c), and the LPS+PNX group (d). *Arrows* indicate area of inflammatory infiltration in the lung. Computed tomography for small animals showed extensive inflation of the remaining right lungs, diaphragmatic lobe protrusion into the left pleural cavity, and left-shifted mediastinum in the groups with pneumonectomy (c and d). The area of lung infiltration was more extensive in the LPS+PNX group (d) than in the LPS group (b).

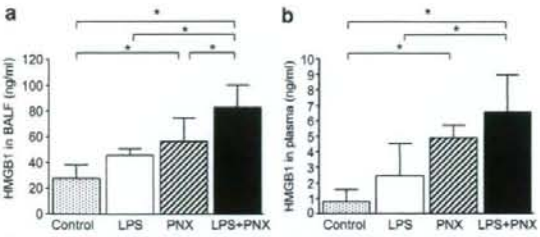

Fig. 6. (a) High mobility group box 1 protein (HMGB1) concentration in bronchoalveolar lavage fluid (BALF). (b) HMGB1 concentration in plasma. HMGB1 increased significantly in both BALF and plasma of the PNX group compared to the control group. Values are means ± S.D.; $n = 6$. *$P < 0.05$. Scheffe's post-hoc test.

3.6. HMGB1 increased in both BALF and plasma of the pneumonectomy group

HMGB1 increased significantly in both BALF and plasma of the PNX group (55.11 ± 15.43 and 4.91 ± 0.82 ng/ml, respectively) and of the LPS+PNX group (79.10 ± 18.43 and 6.57 ± 2.40 ng/ml, respectively), but not of the LPS group (44.42 ± 5.94 and 2.43 ± 2.09 ng/ml, respectively), compared to the control group (32.23 ± 12.5 and 0.79 ± 0.77 ng/ml, respectively). There was also a significant difference in HMGB1 in both BALF and plasma between the LPS and the LPS+PNX groups. In the LPS+PNX group, a significant increase in HMGB1 was observed in BALF, not in plasma, compared with the PNX group ($P < 0.05$) (Fig. 6).

3.7. Increased cytokine levels in BALF after pneumonectomy and/or LPS instillation

Pneumonectomy and/or intratracheal LPS instillation induced significant increases in the levels of six cytokines examined in BALF at 24 h after the insults. Although the BALF level of IFN-γ was increased after pneumonectomy alone compared to the control group (0.47 ± 0.32 vs. 1.24 ± 0.24 pg/ml, $P < 0.05$), there was no significant difference in the level of other five cytokines between the control and the PNX group. LPS instillation alone significantly increased BALF levels of IL-1β, IFN-γ and TNF-α compared to the control group, but the increase in IL-6, IL-10 and KC levels were not significant. There were significant increases in the levels of IL-1β, IL-6, IL-10, IFN-γ, KC and TNF-α in the LPS+PNX group compared to the LPS group and to the control group (Fig. 7).

4. Discussion

Although it is of great interest to a thoracic surgeon what is happening in the residual lung after pulmonary resection, little is known about this information. In the present study, pneumonectomy caused neutrophil and macrophage infiltration, capillary hyperpermeability and edematous changes in the residual lung, which was associated with a significant increase in the plasma and BALF levels of HMGB1, indicating occult injury to the residual lung. Pretreatment with a low dose of LPS induces a greater increase in HMGB1 in the BALF collected from the residual lung, resulting in more severe lung injury. BALF levels of pro-inflammatory cyto-

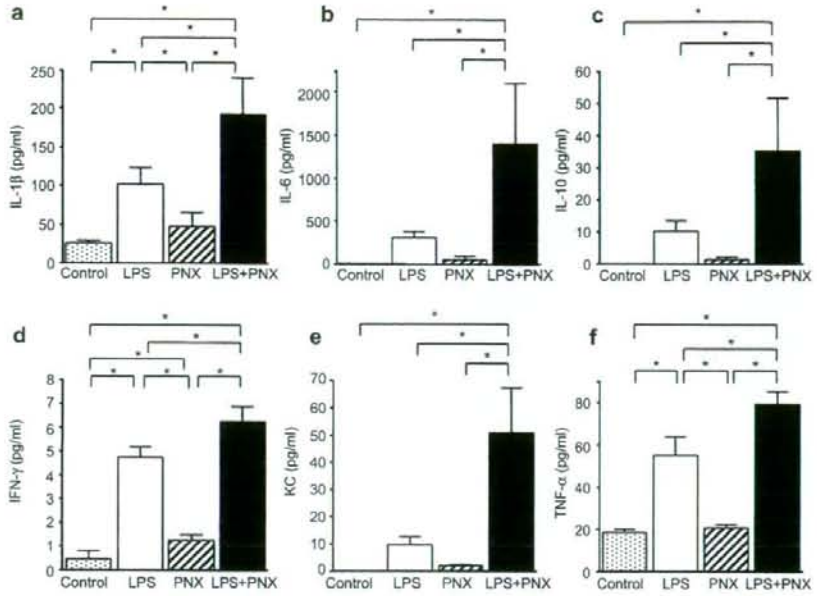

Fig. 7. Bio-Plex bead assay of six major cytokine profiles in bronchoalveolar lavage fluid (BALF). Bio-Plex mouse cytokine assay for simultaneous quantitation of interleukin IL-1β (a), IL-6 (b), IL-10 (c), interferon (IFN)-γ (d), keratinocyte-derived chemokine (KC) (e) and tumor necrosis factor (TNF)-α (f) was used according to the recommended procedure. Values are means±S.D.; $n=6$. *$P<0.05$. Scheffe's post-hoc test.

kines were also increased significantly in a complex response to the combined insult of pneumonectomy and LPS administration. Although our model does not closely approximate the clinical situation, similar mechanisms may underlie ALI/ARDS after lung resection in patients complicated by bacterial infection.

Since, in preliminary experiment, mice recovered quickly after pneumonectomy, and survived long-term (data not shown), we hypothesized that the occult lung injury in the residual lung after pneumonectomy does not affect the outcome unless other factors such as infection take place. To test this hypothesis, we evaluated lung injury after pneumonectomy, with or without low dose LPS administration.

In our experiment, the amount of LPS administered into the lung was half the amount which has been described in previous reports of LPS-induced acute lung injury [13]. This was because, in our preliminary experiments, none of the mice in the LPS+PNX group survived for 24 h when using the same amount of LPS as in the previous reports. We therefore reduced the amount of LPS so that all the mice could survive for longer than 24 h after pneumonectomy and LPS instillation. This may be why in the LPS group neither the permeability index nor the W/D weight ratio increased significantly compared with the control group. However, this low dose of LPS caused a significant increase in both the permeability index and the W/D weight ratio when combined with pneumonectomy. The numbers of neutrophils, macrophages and total cells also increased significantly in the LPS+PNX group compared to the LPS group. Histologically, the most severe lung injury was observed in the LPS+PNX group.

HMGB1 has been shown to play an important role in hemorrhagic shock and ventilator induced lung injury (VILI) [16, 18]. In the present study, the level of HMGB1 increased 1.5-fold in the lung and 5-fold in the plasma at 24 h after pneumonectomy. HMGB1 can be passively released by necrotic or damaged cells when the integrity of cytoplasmic membranes is lost [10]. Although it remains unclear whether mechanical stress induces the release of HMGB1, overinflation might be a stimulus to release HMGB1 in VILI and pneumonectomy models [16]. Overinflation may cause lung tissue damage with HMGB1 release into the bloodstream. HMGB1 in the lung may be released not only from the damaged cells but also from the increased numbers of activated neutrophils and macrophages [10]. Overinflation of the lung causes enlarged intercellular gaps between endothelial and/or epithelial cells, and neutrophils and macrophages may transmigrate into the alveolar space through the enlarged gaps. Otherwise, because pulmonary resection causes tissue damage at the hilar region and the chest wall, HMGB1 may be released into the bloodstream from the damaged cells, which may cause a catabolic state and a systemic inflammatory response in the mice [23, 24].

Although there was no significant difference in HMGB1 levels in BALF and plasma between the control and the LPS groups, HMGB1 levels increased significantly after the combined insults of LPS and pneumonectomy. Since both pneumonectomy and LPS instillation could be a stimulus that induces the release of HMGB1, they could cooperatively have a prominent role [10, 13].

Endotoxemia and severe hemorrhage are not routinely observed following surgical procedures such as pneumonectomy, indicating that other mediators may also contribute

to the inflammatory response that may lead to ALI or multiple organ dysfunctions. HMGB1 has been demonstrated to be an important mediator of mortality and organ system dysfunction, including ALI [10, 13–17]. Suda et al. reported that, in a clinical setting of thoracic esophagotomy, postoperative serum HMGB1 level was higher in patients who developed complications than in those who did not [19]. They concluded that an elevated serum HMGB1 level may contribute to the development of postoperative organ system dysfunction. They also indicated that serum HMGB1 level before the operation may predict the postoperative clinical course. In our experiment, the increased HMGB1 could be one of the mediators which enhance the inflammatory response after pneumonectomy.

Pulmonary hyperpermeability was seen in the remaining lung after pneumonectomy, and the lung W/D weight ratio increased significantly. It has been reported that HMGB1 directly increases the permeability of enterocyte monolayers, and impairs intestinal barrier function through a mechanism that depends on the formation of nitric oxide and peroxynitrite [25]. Similar effects of HMGB1 on pulmonary epithelial tight junctions might develop interstitial pulmonary edema, besides the pro-inflammatory actions of HMGB1.

Our results showed increasing cytokine levels in the residual lungs 24 h after pneumonectomy. Comparison between the control group and the PNX group indicates a trend of increasing levels of six cytokines, suggesting that pro-inflammatory cytokines including TNF-α, IL-1β, IL-6, IFN-γ, KC in BALF, might be involved in post-pneumonectomy occult lung injury. Moreover, comparisons between the four groups detected significant increases in the level of IFN-γ between the PNX group and the control group. Because IFN-γ is reported to stimulate macrophages in the presence of TNF-α and IL-1β, to actively secrete HMGB1 [10], IFN-γ in particular may contribute to the complex response in the residual lung following the combined insults of LPS and pneumonectomy.

In conclusion, HMGB1, together with pro-inflammatory cytokines may play a prominent role in the establishment of occult lung injury after pneumonectomy, which has a potential to progress to ALI when an additional stimulus such as infection exists. This response of HMGB1 may not be unique to pneumonectomy. Other surgical procedures may also induce an increase in HMGB1 levels in the lungs as well as in other organs.

Acknowledgements

We wish to thank Dr Hiromi Sakai (Faculty of Science and Engineering, Waseda University) for his contribution to the statistical analyses and Dr Tokuhiro Kimura (Department of Pathology, Keio University School of Medicine) for his contribution to the pathological scoring.

References

[1] Watanabe S, Asamura H, Suzuki K, Tsuchiya R. Recent results of postoperative mortality for surgical resections in lung cancer. Ann Thorac Surg 2004;78:999–1002; discussion 1002–1003.

[2] Wright G, Manser RL, Byrnes G, Hart D, Campbell DA. Surgery for non-small cell lung cancer: systematic review and meta-analysis of randomised controlled trials. Thorax 2006;61:597–603.

[3] Grichnik KP, D'Amico TA. Acute lung injury and acute respiratory distress syndrome after pulmonary resection. Semin Cardiothorac Vasc Anesth 2004;8:317–334.

[4] Dulu A, Pastores SM, Park B, Riedel E, Rusch V, Halpern NA. Prevalence and mortality of acute lung injury and ARDS after lung resection. Chest 2006;130:73–78.

[5] Kutlu CA, Williams EA, Evans TW, Pastorino U, Goldstraw P. Acute lung injury and acute respiratory distress syndrome after pulmonary resection. Ann Thorac Surg 2000;69:376–380.

[6] Jordan S, Mitchell JA, Quinlan GJ, Goldstraw P, Evans TW. The pathogenesis of lung injury following pulmonary resection. Eur Respir J 2000; 15:790–799.

[7] Bigatello LM, Allain R, Gaissert HA. Acute lung injury after pulmonary resection. Minerva Anestesiol 2004;70:159–166.

[8] Goodwin GH, Sanders C, Johns EW. A new group of chromatin-associated proteins with a high content of acidic and basic amino acids. Eur J Biochem 1973;38:14–19.

[9] Yamada S, Maruyama I. HMGB1, a novel inflammatory cytokine. Clin Chim Acta 2007;375:36–42.

[10] Wang H, Bloom O, Zhang M, Vishnubhakat JM, Ombrellino M, Che J, Frazier A, Yang H, Ivanova S, Borovikova L, Manogue KR, Faist E, Abraham E, Andersson J, Andersson U, Molina PE, Abumrad NN, Sama A, Tracey KJ. HMG-1 as a late mediator of endotoxin lethality in mice. Science 1999;285:248–251.

[11] Blackwell TS, Blackwell TR, Holden EP, Christman BW, Christman JW. In vivo antioxidant treatment suppresses nuclear factor-kappa B activation and neutrophilic lung inflammation. J Immunol 1996;157:1630–1637.

[12] Park JS, Gamboni-Robertson F, He Q, Svetkauskaite D, Kim JY, Strassheim D, Sohn JW, Yamada S, Maruyama I, Banerjee A, Ishizaka A, Abraham E. High mobility group box 1 protein interacts with multiple Toll-like receptors. Am J Physiol Cell Physiol 2006;290:C917–C924.

[13] Ueno H, Matsuda T, Hashimoto S, Amaya F, Kitamura Y, Tanaka M, Kobayashi A, Maruyama I, Yamada S, Hasegawa N, Soejima J, Koh H, Ishizaka A. Contributions of high mobility group box protein in experimental and clinical acute lung injury. Am J Respir Crit Care Med 2004;170:1310–1316.

[14] Andersson U, Wang H, Palmblad K, Aveberger AC, Bloom O, Erlandsson-Harris H, Janson A, Kokkola R, Zhang M, Yang H, Tracey KJ. High mobility group 1 protein (HMG-1) stimulates proinflammatory cytokine synthesis in human monocytes. J Exp Med 2000;192:565–570.

[15] Goto T, Ishizaka A, Kobayashi F, Kohno M, Sawafuji M, Tasaka S, Ikeda E, Okada Y, Maruyama I, Kobayashi K. Importance of tumor necrosis factor-alpha cleavage process in post-transplantation lung injury in rats. Am J Respir Crit Care Med 2004;170:1239–1246.

[16] Ogawa EN, Ishizaka A, Tasaka S, Koh H, Ueno H, Amaya F, Ebina M, Yamada S, Funakoshi Y, Soejima J, Moriyama K, Kotani T, Hashimoto S, Morisaki H, Abraham E, Takeda J. Contribution of high-mobility group box-1 to the development of ventilator-induced lung injury. Am J Respir Crit Care Med 2006;174:400–407.

[17] Suda K, Kitagawa Y, Ozawa S, Saikawa Y, Ueda M, Ebina M, Yamada S, Hashimoto S, Fukata S, Abraham E, Maruyama I, Kitajima M, Ishizaka A. Anti-high-mobility group box chromosomal protein 1 antibodies improve survival of rats with sepsis. World J Surg 2006;30:1755–1762.

[18] Kim JY, Park JS, Strassheim D, Douglas I, Diaz del Valle F, Asehnoune K, Mitra S, Kwak SH, Yamada S, Maruyama I, Ishizaka A, Abraham E. HMGB1 contributes to the development of acute lung injury after hemorrhage. Am J Physiol Lung Cell Mol Physiol 2005;288:L958–L965.

[19] Suda K, Kitagawa Y, Ozawa S, Saikawa Y, Ueda M, Abraham E, Kitajima M, Ishizaka A. Serum concentrations of high-mobility group box chromosomal protein 1 before and after exposure to the surgical stress of thoracic esophagectomy: a predictor of clinical course after surgery? Dis Esophagus 2006;19:5–9.

[20] Sakurai MK, Greene AK, Wilson J, Fauza D, Puder M. Pneumonectomy in the mouse: technique and perioperative management. J Invest Surg 2005;18:201–205.

[21] Mrozek JD, Smith KM, Bing DR, Meyers PA, Simonton SC, Connett JE, Mammel MC. Exogenous surfactant and partial liquid ventilation: physiologic and pathologic effects. Am J Respir Crit Care Med 1997;156: 1058–1065.

[22] Yamada S, Inoue K, Yakabe K, Imaizumi H, Maruyama I. High mobility group protein 1 (HMGB1) quantified by ELISA with a monoclonal antibody that does not cross-react with HMGB2. Clin Chem 2003;49:1535–1537.

[23] Craig SR, Leaver HA, Yap PL, Pugh GC, Walker WS. Acute phase responses following minimal access and conventional thoracic surgery. Eur J Cardiothorac Surg 2001;20:455–463.

[24] Leaver HA, Craig SR, Yap PL, Walker WS. Lymphocyte responses following open and minimally invasive thoracic surgery. Eur J Clin Invest 2000;30:230–238.

[25] Sappington PL, Yang R, Yang H, Tracey KJ, Delude RL, Fink MP. HMGB1 B box increases the permeability of Caco-2 enterocytic monolayers and impairs intestinal barrier function in mice. Gastroenterology 2002;123:790–802.

Modern Pathology (2008) 21, 992–1001

www.modernpathology.org

Histopathological features and prognostic significance of the micropapillary pattern in lung adenocarcinoma

Kazunori Kamiya[1,2], Yuichiro Hayashi[1], Junya Douguchi[1], Akinori Hashiguchi[1], Taketo Yamada[1], Yotaro Izumi[2], Masazumi Watanabe[2], Masafumi Kawamura[2], Hirohisa Horinouchi[2], Naoki Shimada[3], Koichi Kobayashi[2] and Michiie Sakamoto[1]

[1]*Department of Pathology, School of Medicine, Keio University, Tokyo, Japan;* [2]*Department of Surgery, Division of General Thoracic Surgery, School of Medicine, Keio University, Tokyo, Japan and* [3]*Department of Preventive Medicine and Public Health, School of Medicine, Keio University, Tokyo, Japan*

The micropapillary pattern is characterized by small papillary tufts with no fibrovascular core lying in spaces and has been reported as an aggressive variant of carcinoma in several organs. We investigated the histopathobiological properties of the micropapillary pattern with immunohistochemistry, serial sections, and electron microscopy in lung adenocarcinoma. We further analyzed its clinicopathological character and prognosis. The subjects included 383 adenocarcinoma cases, of which 184 (48%) were micropapillary pattern-positive and 199 (52%) were micropapillary pattern-negative. On histology, micropapillary tufts seemed to float in the alveolar space or spaces encased by connective tissues, whereas serial sections revealed that most tufts had continuity with other tufts and even with the main tumor. Positive staining for the adhesion molecules E-cadherin and β-catenin suggested the preservation of tight adhesion, and electron microscopy showed the existence of intercellular junctions. Negative staining for laminin and loss of basement membrane as determined by electron microscopy suggest a loss of cell–matrix contact. Positive staining for Ki-67 indicates that cells constituting micropapillary tufts retained their proliferation potency. There were no CD34-positive cells in micropapillary tufts, and the loss of the vascular core was confirmed. In micropapillary pattern-positive cases, lymphatic invasion was identified significantly more frequently than in micropapillary pattern-negative cases ($P<0.001$), even at stageIA (without lymph node metastasis, $N=197$) ($P<0.001$). The 5-year and 10-year overall survival rates of the micropapillary pattern-positive stageIA group were 77.6 and 67.6%, respectively, which were significantly less than those of the micropapillary pattern-negative stageIA group (98.1 and 98.1%) ($P=0.001$). In conclusion, cells constituting the micropapillary pattern are likely to have acquired anchorage-independent growth and a potential for high malignancy.
Modern Pathology (2008) **21**, 992–1001; doi:10.1038/modpathol.2008.79; published online 30 May 2008

Keywords: lung adenocarcinoma; micropapillary pattern; histopathology; prognosis; immunohistochemistry; electron microscopy

Introduction

Lung cancer is one of the most common causes of cancer-related death worldwide.[1] The prognosis of patients with lung cancer is generally poor, and the overall 5-year survival rate is 15%.[2] Of the four main histological types of lung cancer, adenocarcinoma is increasing in frequency and accounts for almost half of all lung cancers.[3] Recent advances in diagnostic imaging have enhanced the capability for diagnosis at the early stage, and histopathological studies indicate the existence of good prognostic groups in lung cancer. Bronchioloalveolar carcinoma, defined as a non-invasive subtype of lung adenocarcinoma,[3] is recognized as ground-glass opacity lesion on computed tomography and is reported to have a good prognosis.[4] However, the overall 5-year survival of patients with stageIA (T1N0M0: T1, tumor greatest dimension ≤30 mm and surrounded by pleura; N0, no regional lymph node metastasis; M0, no distant metastasis)[5] adenocarcinomas does not reach 80%,[6,7] which indicates the existence of a poor prognostic group. Factors including smoking history, serum level of carcinoembryonic antigen, and tumor size, as well as lymphatic and venous

Correspondence: Dr M Sakamoto, MD, Department of Pathology, School of Medicine, Keio University, 35 Shinano-machi, Shinjyuku-ku, Tokyo 160-8582, Japan.
E-mail: msakamot@sc.itc.keio.ac.jp
Received 03 January 2008; revised 16 April 2008; accepted 17 April 2008; published online 30 May 2008

invasion have been identified as poor prognostic factors for lung adenocarcinoma.[8–12]

Recently, a pathological entity called the micropapillary pattern has been reported to have worse outcomes in breast,[13] colon,[14] urinary tract,[15] ovary,[16] salivary gland,[17] and lung[18,19] cancer. The micropapillary pattern in lung adenocarcinoma is characterized by small papillary tufts lying in alveolar spaces or in spaces encased by connective tissues, with the tufts having no fibrovascular core,[18,19] and it has been reported as an important factor for poor prognosis.[18–21] However, the detailed histopathobiological features of the micropapillary pattern have not yet been clarified. We investigated the histological, immunohistochemical, electron microscopic, and clinicopathological properties of the micropapillary pattern to elucidate why it could be a factor in poor prognoses.

Materials and methods

Surgical Specimens and Patient Characteristics

From January 1993 to December 2006 in Keio University Hospital, 526 patients underwent complete surgical resection of lung cancer diagnosed as primary lung adenocarcinoma. We reviewed these sections macroscopically and microscopically as mentioned below. The histological type of the tumor was described according to the World Health Organization classification[3] and pathological staging was performed according to the classification of the Union Internationale Coutre le Cancer.[3] Because bronchioloalveolar carcinoma has been defined as a non-invasive lesion[3] and there was no existence of the micropapillary pattern in cases composed only of bronchioloalveolar carcinoma ($N=68$), we excluded these cases from clinicopathological analysis. For accuracy of survival analysis, stageIIIB and stageIV cases with the possibility of incomplete resection were excluded as well. Therefore, the final population for clinicopathological analysis consisted of 383 cases (214 men and 169 women ranging from 29 to 85 years of age, with an average age of 62.3 years). Clinicopathological information was obtained by reviewing the medical charts in detail with regard to age (<60 or ≥ 60 years), sex (male or female), smoking history (nonsmoker or smoker: smoker was defined as more than 1 year of smoking history), recurrence, and survival. The follow-up period ranged from 3 to 158 months (mean was 60.9 months). This study was conducted under the approval of the Ethics Committee of the Keio University School of Medicine.

Histological Examination

Surgically resected specimens were fixed routinely in 10% formalin, cut serially into 5- to 7-mm-thick slices, and macroscopically examined. From the section including the maximum tumor diameter, all the tumor tissues as well as the surrounding lung tissue were removed and embedded in paraffin, and then cut into 4-μm-thick sections. Finally, hematoxylin–eosin and Elastica Van Gieson staining were performed and all sections for each patient were observed. The following histopathological factors were evaluated: tumor size (maximum tumor diameter ≤ 30 or >30 mm), lymph node metastasis, pleural invasion, lymphatic invasion, and venous invasion. The histological patterns were divided into four distinctive subtypes: bronchioloalveolar carcinoma as well as acinar, papillary, and solid adenocarcinoma with mucin; the latter three subtypes were defined as invasive.[3] The dominant subtype of each tumor was then documented.

The micropapillary pattern was defined according to the two previous studies;[18,19] it was identified as small tufts lying in alveolar spaces or in spaces encased within thin walls of connective tissue, and the tufts had no fibrovascular core. The extent of the micropapillary pattern was subclassified as none (0% of the tumor), focal ($<10\%$), moderate ($<50\%$), or extensive ($\geq 50\%$) based on the proportion of micropapillary pattern area in the tumors.

Furthermore, three micropapillary pattern-positive samples (extent: moderate and extensive) were selected and 100 serial sections stained by hematoxylin–eosin were then examined sequentially at intervals of 12 μm with attention paid to the morphology of the micropapillary pattern.

Immunohistochemistry

For immunohistochemistry, 20 cases of tumor with the micropapillary pattern were randomly selected and studied (10 cases with lymph node metastasis and 10 without).

Four-micrometer-thick sections were deparaffinized, rehydrated, and incubated in 0.03% H_2O_2 in 95% methanol at room temperature for 20 min to block the endogenous peroxidase activity. Autoclave pretreatment at 120°C for 10 min in 10 mM citrate buffer (pH 6.0) was used for E-cadherin and Ki-67 antigen retrieval. Water bath pretreatment at 100°C for 10 min in 10 mM citrate buffer (pH 9.0) was used for β-catenin and CD34 antigen retrieval. Incubation in 4 mg/ml pepsin (Dako, Glostrup, Denmark) in 0.2 N HCl at 37°C for 60 min was used for laminin antigen retrieval. All sections were incubated for 20 min with normal horse serum to eliminate nonspecific staining and then incubated with the following primary antibodies: anti-human E-cadherin (1:200; Novocastra Laboratories, Newcastle, UK), anti-human β-catenin (1:200; Santa Cruz Technology, Santa Cruz, CA, USA), anti-human laminin (1:400; Dako), anti-human CD34 (1:100, Dako), and anti-human Ki-67 (diluted at 1:400; Dako). These antibodies were applied overnight at 4°C, followed by incubation with the secondary antibody

(ImmPRESS™ Reagent Kit, Vector Laboratories, Burlingame, CA, USA) for 30 min. Slides were then incubated in DAB/Tris solution (three DAB/Tris tablets diluted in 150 ml distilled water; Muto Pure Chemicals, Tokyo, Japan) supplemented with 15 μl of 30% H_2O_2. Finally, the slides were counterstained with hematoxylin. Ki-67 expression was evaluated by counting 400 tumor cells in 4 high-power fields (× 200) from the micropapillary pattern areas in all 20 cases, and expressed as the percentage nuclear-stained cells.

Electron Microscopy

Three tumor specimens, already fixed with formalin and diagnosed as adenocarcinoma with the micropapillary pattern (extent: moderate and extensive), were selected and studied. Specimens were refixed in 2.5% glutaraldehyde in an isomolar phosphate buffer (pH 7.4), postfixed in 1% osmium tetroxide for 1.5 h, dehydrated in graded alcohol, and embedded in Epon 812. Ultrathin sections were mounted on copper grids, stained with uranyl acetate and lead citrate, and then examined with a JEM-1200 transmission electron microscope (Nihon Denshi, Tokyo, Japan).

Statistical Analysis

The length of disease-free survival was defined as the period from the date of surgery to the date when recurrence was diagnosed, and that of overall survival was defined as the period until the date of either death as a result of the tumor or the most recent follow-up. Survival curves were plotted using the Kaplan–Meyer method and *P*-values were calculated using the log-rank test. The correlations between several clinicopathological characteristics and histological subgroups were evaluated using the χ^2 test. *P*-values of less than 0.05 were accepted as significant. Data were analyzed with Statistical Standard Package Service Solution software (SPSS for Standard version 15.0; SPSS Inc, Chicago, IL, USA).

Results

Histological Examination

Of the 383 cases of adenocarcinoma, 103 (27%), 69 (18%), 182 (48%), and 29 (7%) were in the dominant bronchioloalveolar carcinoma, acinar, papillary, and solid with mucin subtypes, respectively (Table 1).

On histology, micropapillary tufts had no fibrovascular core and were detected in the alveolar space (Figure 1a), or in spaces inside the tumor that in most cases represented retracted connective tissue (Figure 1b), and adjacent to any of the above-mentioned four histological pattern subtypes. The micropapillary pattern was detected in 184 patients (109 men and 75 women), with 19 (11%), 33 (18%), 117 (63%), and 15 (8%) in the dominant bronchioloalveolar carcinoma, acinar, papillary, and solid with mucin subtypes, respectively (Table 1).

The extent of the micropapillary pattern present in tumors varied. The numbers of patients with focal, moderate, and extensive were 65 (35%), 85 (46%), and 34 (19%), respectively.

In the three cases studied using serial sections, we found that most tufts had continuity with other tufts and main tumor. For example, a tuft marked by (➡) in section 12 was consecutive with another tuft in section 8 and with the main tumor in section 1. Two isolated tufts, identified by (➔) in section 4, were shown to be consecutive in section 10. There also existed several tufts lacking continuity with any other tuft. The tuft marked by (→) in sections 5, 6, and 7 could not be confirmed to be continuous with any other tuft (Figure 2). Micropapillary tufts were observed to present an intricate morphology.

Immunohistochemical Findings

E-cadherin was positive at intercellular cell membranes in every micropapillary tuft, and showed no difference in staining intensity when compared with neoplastic cells in the main tumor (Figure 3a). β-Catenin staining showed the same pattern as E-cadherin (Figure 3b). Tight adhesion of cells constituting micropapillary tufts was therefore believed to be maintained. Laminin was identified in the basement membrane of normal alveolar cells and neoplastic cells of the main tumor, but on the other hand, it was not found in any cell constituting micropapillary tufts (Figure 3c). It is most likely that cells constituting micropapillary tufts had no basement membrane and therefore showed disordered continuity with the matrix. Cells constituting micropapillary tufts appeared to pile up. CD34-positive cells were enriched in the stroma of the main tumor and in the alveolar septum, whereas no CD34-positive cells were found in any micropapillary tuft (Figure 3d). No vascularity was observed in micropapillary tufts. These findings were confirmed in all 20 cases. Differences in staining pattern and intensity between cases with and without lymph node metastasis ($N = 10$ each) were not found. To determine whether cells composing micropapillary tufts had proliferation potency, Ki-67 staining was performed. Cells constituting micropapillary tufts showed positive staining for Ki-67 (Figure 3e); positive rates ranged from 5 to 45% with a mean of 20.3%. Cells constituting micropapillary tufts were therefore believed to have proliferation potency.

Electron Microscopy

Electron microscopy showed no basement membrane or vascular structures. Microvilli were some-